Astronomical and Astrophysical Transactions (*AApTr*), 2017, Vol. 30, Issue 2, pp. 173–184,
ISSN 1055-6796, Photocopying permitted by license only, ©Cambridge Scientific Publishers

The saturation state of H_2O masers in star forming regions

V.S. Strelnitski[1,*], B.P. Holder[1], V.I. Shishov[2], N.I. Nezhdanova[1]

[1] *Maria Mitchell Observatory, Nantucket, MA 02554, USA*
[2] *P.N. Lebedev Physical Institute, Moscow, Russia*

Received 1 March, 2017

This paper is dedicated to the memory of Professor Iosif Samuilovich Shklovsky, one of the pioneers of the studies of natural ("cosmic") masers.

We propose a new approach to answer the question of whether strong H_2O masers in regions of active star formation operate in an unsaturated or saturated regime. The applicability of the approach rests on the assumption that these masers are associated with turbulence. To illustrate the basic idea of the approach, we present an analytical solution for high-gain maser amplification in a single-scale turbulent medium, which shows that the spectra and maps of the masers are qualitatively different in the unsaturated and saturated cases. Then, we develop a numerical model in which a homogeneous and isotropic, Kolmogorov-type, random velocity field is created in a box with 512^3 grid points. The observed fractal structure of maser clusters (likely due to the intermittency of the turbulence) is accounted for by randomly canceling a part of the active cells, so that the remaining part occupies a random fractal set. The model returns integrated spectra and 2D-projection source maps for unsaturated and saturated maser amplification in such a medium. Realizations of the model show that unsaturated (exponential) amplification with gains $\gtrsim$30 (required by the observed brightness temperatures of the bright maser spots) results in a very small number of bright peaks in the spectrum, corresponding to a few isolated hot spots on the map, with no self-similar clustering (fractal structure) of the spots. If the maser is saturated (linear amplification), the output contains many spectral/spatial components of comparable intensity, and the fractal structure is seen through all the scales, down to the smallest groups of elementary cells. Using the spectra and interferometric maps of H_2O masers in W49(N) and Sgr B2(M) for comparison, we show that these observations are better described by the saturated case. We conclude that, if the strong H_2O masers in star forming regions are associated with turbulence, they are most likely saturated.

Keywords: Masers – star formation – turbulence

*Email: strelnitski@yahoo.com

1 Introduction

To know the degree of saturation of bright 22.2 GHz H_2O masers on the 6_{16}–5_{23} rotational transition, observed in regions of active star formation, is crucially important for understanding the origin of their brightness, line width, and polarization. The observed flux densities, together with some indirect estimates of the upper limit on the length of the amplification path, seem to require heavy saturation, in order for observations to be explained by the proposed pumping mechanisms (Strelnitskii 1984). The high degree of linear polarization observed in some sources also requires a high degree of saturation, if polarization is due to the Zeeman effect in a magnetic filed [e.g., Degouchi & Watson (1986)]. On the other hand, the separation between the major three hyperfine components of the 6_{16}–5_{23} transition being $>1\,\mathrm{km\,s^{-1}}$, the narrowness of some observed spectral features (down to $\approx 0.4\,\mathrm{km\,s^{-1}}$) is more easily explained if the maser is unsaturated [e.g., Strelnitski (1982)].

Here, we investigate the possibility to discriminate between the alternatives of unsaturated and saturated masering of H_2O in regions of star formation, using the hypothesis that these masers (at least those corresponding to the "low-velocity" core of the spectrum) arise in a *turbulent* medium. Arguments in favor of this assumption have been presented several times during the past three decades [e.g., Reid et al. (1988); Strelnitski et al. (2002); Imai et al. (2002); Fish et al. (2011)]. The general conclusion is that strong H_2O masers in star-forming regions participate in regular motions of the gas (e.g., expansion and rotation) around newly-born stars, but that this gas is also turbulent. In Strelnitski et al. (2002), several probable signatures of turbulence were pointed out for a number of sources mapped with VLBI, including: (1) two-point velocity structure functions with exponents near their classic Kolmogorov values for incompressible turbulence; (2) a considerable excess of large two-point velocity increments as compared with a Gaussian distribution about their mean values; and (3) a fractal spatial distribution of maser spots with a dimension $d_0 \lesssim 1$. Fractal geometric structure and an excess of large velocity increments are well-known signatures of *intermittent* turbulence [e.g., Frish (1995)]. Strelnitski et al. (2002) argue that turbulence may in fact be the *cause* of masering, by providing energy for collisional pumping in small-scale stochastic shock waves.

Formulated more concretely, the goal of the present investigation is to see which of the two possible asymptotic regimes of maser amplification – completely unsaturated or totally saturated – is in a better qualitative agreement with the observed spectra and maps of the maser sources within the probable limits of the physical parameters of the sources.

In Section 2 we present an analytical solution of the problem of maser propagation in a homogeneous, isotropic turbulent medium with a simple, single-scale, random velocity field. This solution illustrates the basic idea of our approach, namely, that the output of the maser amplification in a turbulent medium can be qualitatively different for the unsaturated and saturated regimes of amplification. A numerical model with a more realistic presentation of turbulence, in both the physical and the velocity space, is described in Section 3 and the results of simulations (synthetic maps and spectra of saturated and unsaturated maser emission from such a turbulent medium) are compared with VLBI maps and integrated spectra of bright H_2O sources. Our conclusions are summarized in Section 4.

2 Analytical approach

Consider the propagation of maser radiation through a homogeneous, isotropic medium with a single-scale random velocity field. Let $\alpha_\nu^u(\vec{r})$ be the absolute value of the (negative) unsaturated absorption coefficient of the medium for the radiation propagating along the line of sight:

$$\alpha_\nu^u(\vec{r}) = \alpha_0^u \exp\left[-\frac{(\nu-\mu-\nu_0)^2}{(\delta\nu)^2}\right] , \tag{1}$$

where ν is the observed frequency of radiation, $\vec{r}$ is the position vector of the point in the medium, ν_0 is the central frequency of the line in the medium at rest, α_0^u is the absolute value of the unsaturated absorption coefficient in the center of the thermally broadened line, μ is the random Doppler shift of central frequency due to turbulent motions, and $\delta\nu$ is the thermal line width. Under "unsaturated" we understand the absorption coefficient that is determined by all the elementary processes affecting the populations of the signal levels except for the stimulated radiative transitions between these levels [i.e. the situation where the intensity of maser radiation is much lower than the "saturation intensity"; see, for example, Goldreich & Kwan (1974)]. We assume, for the sake of simplicity, that μ is a Gaussian function of $\vec{r}$, with the first two moments

$$\langle\mu\rangle = 0 \tag{2}$$

and

$$\langle\mu(\vec{r_1})\mu(\vec{r_2})\rangle = (\delta\mu)^2 \exp\left(-\frac{r^2}{b^2}\right) , \tag{3}$$

where $r \equiv |\vec{r_1} - \vec{r_2}|$, b is the spatial scale of turbulent velocity variations, and $\delta\mu$ is the standard deviation of the frequency shift due to turbulence. The angle brackets signify averaging over realizations. We assume that $\delta\mu >> \delta\nu$, which makes $\alpha_\nu^u(\vec{r})$ a strongly varying, random function of $\vec{r}$.

The unsaturated optical depth along the line of sight, for a point in the plane of the sky described by a two-dimensional vector $\vec{d}$, is

$$\tau_\nu^u(\vec{d}) = \int_0^L \alpha_\nu^u(\vec{r})\,\mathrm{d}z , \tag{4}$$

where L is the length of the active medium along the line of sight passing through the point $\vec{d}$. By averaging equation (4) over realizations, with an account for the Gaussian nature of μ, we get:

$$\langle\tau_\nu^u\rangle = \frac{\alpha_0^u L}{\sqrt{1+\gamma^2}} \exp\left[-\frac{(\nu-\nu_0)^2}{(\delta\nu)^2\,(1+\gamma^2)}\right] , \tag{5}$$

where $\gamma = \sqrt{2}\delta\mu/\delta\nu$. For $\gamma^2 >> 1$,

$$\langle\tau_\nu^u\rangle \approx t_0^u \exp\left[-\frac{(\nu-\nu_0)^2}{2(\delta\mu)^2}\right] , \tag{6}$$

where $t_0^u \equiv (\alpha_0^u L)/\gamma$. For $\gamma^2 >> 1$, $\langle\tau_0^u\rangle \approx t_0^u$.

An analysis of the correlation function for the fluctuations of τ_ν^u leads to the following equation for the standard deviation of the optical depth:

$$\delta\tau_\nu^u \approx \left[\sqrt{2}\,\ln(2\gamma)\,\frac{b}{L}\right]^{1/2}\langle\tau_\nu^u\rangle\ . \tag{7}$$

The distribution function of the random values of τ_ν^u is Gaussian:

$$f(\tau_\nu^u) = \frac{1}{\sqrt{2\pi}\,\delta\tau_\nu^u}\exp\left[-\frac{(\tau_\nu^u - \langle\tau_\nu^u\rangle)^2}{2\,(\delta\tau_\nu^u)^2}\right]\ . \tag{8}$$

Let us consider two asymptotic cases: (1) the maser is completely saturated at all the frequencies of interest, and (2) the maser is totally unsaturated.

In the completely saturated case, the intensity at a given point $\vec{d}$ and given frequency ν at the maser output changes in direct proportion to the absolute value of the *unsaturated* optical depth of the medium for this output point and frequency. This paradoxically sounding result follows from the solution of the radiative transfer equation for a masering line [see, for example, Eq. (8) in Goldreich & Kwan (1974), in the right-hand side of which the unsaturated absorption coefficient was assumed to be a constant of the propagation path; for a general case, it should be replaced by the integral from our Eq. (4)]. Thus, in the completely saturated case,

$$I_\nu^{\rm s}(z) = I_\nu(0) + {\rm const}\cdot\tau_\nu^u(z)\ , \tag{9}$$

where $I_\nu(0)$ is the intensity of the input radiation. Consequently, the average intensity will be just a scaled version of the averaged optical depth given by Eq. (6), and, with the use of Eq. (7), the fractional dispersion of the output intensity is

$$\frac{\delta I_\nu^s}{\langle I_\nu^s\rangle} \approx \frac{\delta\tau_\nu^u}{\langle\tau_\nu^u\rangle} \approx \left[\sqrt{2}\,\ln(2\gamma)\,\frac{b}{L}\right]^{1/2}. \tag{10}$$

With the plausible estimates of $\gamma \approx 20$ and $b/L \sim 10^{-2}$ for the sources in question, the expected dispersion of intensities is not large, $\delta I_\nu^s/\langle I_\nu^s\rangle \sim 20\%$.

In the unsaturated case, the intensity grows exponentially with $\tau_\nu^u(z)$ [see Eq. (8) in Goldreich & Kwan (1974), with the above comment on its right-hand side]:

$$I_\nu^u(z) = I_\nu(0)\cdot\exp\left[\tau_\nu^u(z)\right]\ . \tag{11}$$

Using the Gaussian character of $\tau_\nu^u(z)$, we get the following equation for the average intensity:

$$\langle I_\nu^u\rangle \approx I_\nu^u(0)\exp\left[\langle\tau_\nu^u\rangle + \frac{1}{2}(\delta\tau_\nu^u)^2\right]\ . \tag{12}$$

It is seen from this equation that when $\delta\tau/\langle\tau\rangle$ is not small, the main contribution to the average intensity is provided by realizations of τ that are considerably greater than $\langle\tau\rangle$.

This is illustrated in Fig. 1, where $\tau \equiv \tau_0^u$. Besides the graph of e^τ, this figure shows the graphs of $f(\tau)$ and $f(\tau)\cdot\mathrm{e}^\tau$ for the case $\gamma = 20$, $b/L = 0.012$, and $\langle\tau_0^u\rangle \approx t_0^u = 20$. According to Eq. (7), these parameters imply $\delta\tau \approx 5$, and thus the argument

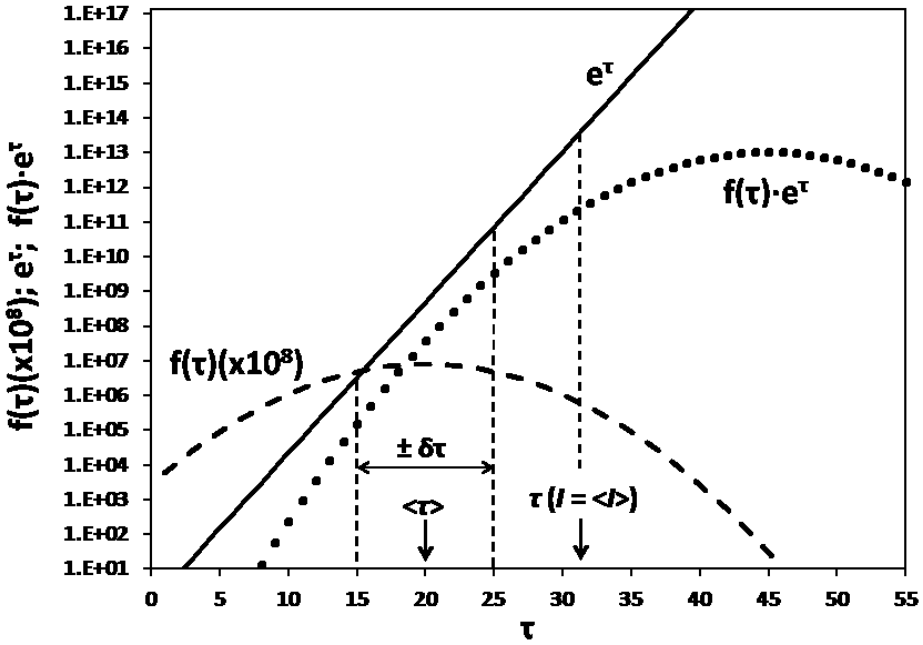


Figure 1 To the explanation of the analytical model (single-scale turbulence with $\gamma = 20$, $\langle\tau\rangle = 20$ and $b/L = 0.012$).

of $\langle I\rangle$, $[\langle\tau\rangle + 0.5\,(\delta\tau)^2] \approx 32.5$. The vertical arrows in Fig. 1 show this value and the value of $\langle\tau\rangle = 20$. The dashed vertical lines projected up to the graph of e^τ show that the average intensity for such a source is several orders of magnitude higher than the intensities corresponding to the bulk of realizations – those falling into the interval $\pm\delta\tau$ from $\langle\tau\rangle$ ($\approx 3/4$ of all realizations). The high value of $\langle I\rangle$ is caused by the less probable realizations of larger values of τ, around $\tau \approx \langle\tau\rangle + 0.5\,(\delta\tau)^2$. One can expect, therefore, that a high-gain, turbulent unsaturated maser source will exhibit a small number of relatively very bright spots, created by those rare lines of sight that happened to acquire τ values considerably higher than $\langle\tau\rangle$. We emphasize that these effects are only expected for sources with sufficiently high values of $\langle\tau_0^u\rangle \approx t_0^u$. The typical observed brightness temperatures of bright H_2O masers, $T_b \sim 10^{12} \to 10^{15}$ K [e.g., Gwinn (1994)], require unsaturated maser gains $\tau \gtrsim 30$ which is comparable to the gain corresponding to the average intensity in the model shown in Fig. 1.

In summary: for a turbulent maser source with the maximum unsaturated gain $\gtrsim$30, one expects very different integrated spectra and maps in the saturated and unsaturated regimes of amplification. In the saturated regime, the map should contain a large number of spots with comparable brightness and the integrated spectrum should be filled with features of comparable intensity whose envelope is approximately Gaussian with the "turbulent width," $\delta\mu$. In the unsaturated case, one expects a map with a small number of bright spots and an integrated spectrum containing, correspondingly, a small number of bright single features.

3 Numerical approach

3.1 The model

We verify our analytical results using a numerical model in which the simulated turbulent velocity field is more realistic, corresponding to fully developed, intermittent turbulence – the medium has a Kolmogorov velocity spectrum, with turbulent activity limited to a fractal spatial structure. After creating such a velocity field numerically, in a 512^3 grid point box, we calculate the x–y distribution of the optical depth along the z-direction (the "line-of-sight") and the output maser intensity distribution, using the assumptions of both saturated and unsaturated amplification regime. The average two-point velocity increment at the largest spatial scale is taken to be approximately 20 times greater than the speed of sound, which is typical for VLBI maps of "low-velocity" H_2O masers in regions of star formation. Although this implies that the velocity field is highly supersonic, the statistical properties of observed maser velocities are typically close to those of incompressible turbulence (Strelnitski et al. 2002; Imai et al. 2002). Therefore, we adopt the well-known Kolmogorov power spectrum for incompressible turbulence for the model velocity field.

We implement a slightly simplified version of the procedure introduced by Dubinski, Narayan & Phillips (1995), where the velocity field in physical space is obtained by taking the inverse Fourier transform of a random field in the wave-number (k) space. Since we are interested only in maser amplification along the line of sight (which we choose to be parallel to the z-axis) we limit the calculation to only the v_z component of the velocity field. In contrast to Dubinski, Narayan & Phillips (1995), we omit the preliminary step of determining the k-space velocity field from a randomly generated vector potential, and instead generate the random field $v_z(\vec{k})$ directly from the assumption of a Kolmogorov energy spectrum:

$$P_v(k) \equiv \langle |v_z(\vec{k})|^2 \rangle \propto k^{-\frac{11}{3}} , \tag{13}$$

where $k \equiv |\vec{k}|$. The use of a vector potential guarantees that the numerically created turbulence is strictly incompressible, but, since we specify only a single component of the velocity field, this restriction is unnecessary. In what follows, we suppress the z subscript on the velocity.

The steps for creating the turbulent vector field are as follows:

1. Create a complex 512x512x512 array of $v(\vec{k}) = |v(\vec{k})|e^{i\phi(\vec{k})}$, with the symmetry property $v(-\vec{k}) = v^\star(\vec{k})$. The magnitudes $|v(\vec{k})|$ are assigned randomly from a Gaussian distribution with zero mean and variance $\sigma^2 = \langle |v(\vec{k})|^2 \rangle = Ck^{-\frac{11}{3}}$. The real constant C is selected to obtain the appropriate range of the physical velocities. Complex phases are selected randomly from a uniform distribution $\phi_i \in [0, 2\pi]$.

2. Apply the three-dimensional Fast Fourier Transform (FFT) to this complex array to obtain a real three-dimensional array of the velocities in physical space.

3. Adjust the constant C to achieve reasonable values for the velocities in physical space.

To reproduce the observed fractal structure of the H_2O masers, likely due to the intermittency of the underlying turbulence, we use the relation between the fractal dimension of a set, d, and its running filling factor, β [e.g., Frish (1995)]:

$$d = d_0 - \frac{\ln\beta}{\ln s} \ , \tag{14}$$

where $d_0 = 3$ is the dimension of the supporting space and s is the scaling factor.

We adopt $s = 1/2$ and $\beta = 1/4$, meaning that the original cube is divided into 8 sub-cubes with two randomly chosen to be "active". Then we subdivide each of the two active sub-cubes into 8 cubes, randomly choose two of them, and continue this procedure down to the smallest scale. Thus, 512 elementary cells, distributed over a random fractal set with dimension $d = 1$ [see Eq. (14)], are retained and contribute to the radiation transfer. This fractal dimension is somewhat higher than in most of the observed H_2O maser sources, but the limited resolution of our model makes it difficult to create a lower fractal dimension using this method.

Once a random sample of the velocity field has been created, we compute the absolute value of the line-of-sight optical depth (the maser gain), τ, for each elementary column with coordinates (x, y), and at every grid value of the "observed" radial velocity, v, in the synthetic spectrum under construction:

$$\tau(x, y, v) = \tau_1 \sum_i \exp\left[-\frac{(v - v^i_{\rm turb})^2}{v^2_{\rm th}}\right] \ , \tag{15}$$

where τ_1 is the gain of an elementary cell, and $v_{\rm th}$ is the dispersion of thermal velocities. The maser intensity of each column, as a function of velocity, is then calculated using the assumption of completely saturated or totally unsaturated amplification [equations (9) and (11), respectively]. For our computations, we assume the constant to be unity in both Eq. (9) and (11).

To properly compare the computed and observed spectra and maps for an unsaturated maser, the observational requirement of maximum gains to be $\tau_{max} \gtrsim 30$ was satisfied by an adjustment of the elementary value of optical depth, τ_1. Since in the saturated case $I \propto \tau$, the spectral intensity distribution of I is a scaled spectral distribution of τ, and therefore τ_1 can be arbitrary in this case.

The typical dynamical range of intensities in the observed spectra of strong H_2O masers is 2–4 orders of magnitude. To account for this, we throw out (call unobservable) all columns with output intensities <0.001 of the highest value at each computational frequency.

3.2 The results of simulations

Figures 2–5 show the results of representative random realizations for saturated and unsaturated maser amplification.

The integrated spectrum and the map for saturated amplification (Figs 2 and 3, left) are drastically different from those for unsaturated amplification (Figs 2 and 3, right).

In the saturated case, there are many hot spots of comparable intensity in the output plane and they are organized in random clusters of different scales; the spectrum

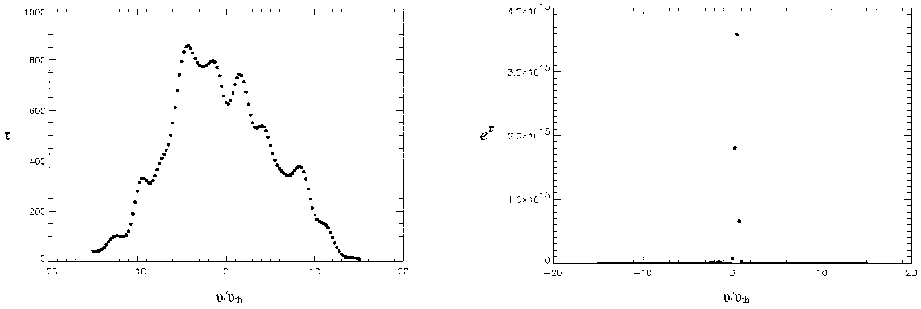


Figure 2 Synthetic spectra of maser emission from a turbulent medium with $\langle v_z^2 \rangle = (20\, v_{\rm th})^2$ for saturated amplification (*left*) and unsaturated amplification with $\tau_{\rm max} \approx 36$ (*right*).

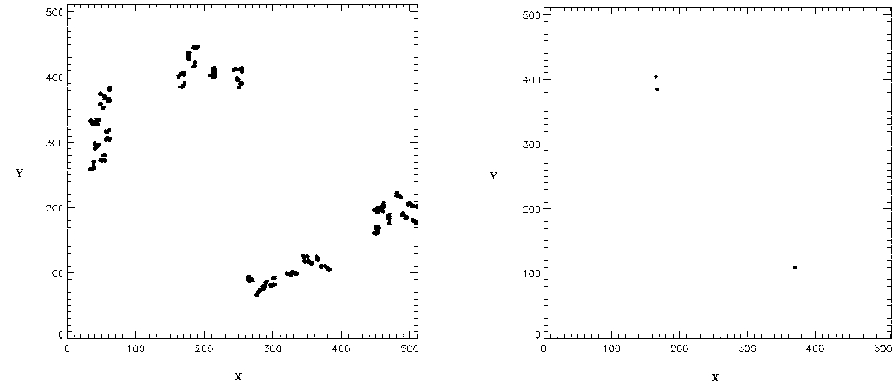


Figure 3 The (x, y) maps of saturated $(left)$ and unsaturated $(right)$ maser emission for the same realizations of turbulent medium as in Fig. 2.

occupies the whole range of turbulent velocities and is filled with overlapping features of comparable intensity. In the unsaturated case, the spectrum consists of one very bright narrow feature and two relatively weak features (barely seen in Fig. 2, right), and the map (Fig. 3, right) shows the three corresponding hot spots.

Zooming in on the clusters of the saturated map (Fig. 4, left) reveals a random fractal structure, down to the smallest scales. We computed the fractal dimension of the saturated model map using the density-radius method [see details in Strelnitski et al. (2002)]:

$$d = \frac{d(\log \Sigma)}{d(\log r)} \ , \tag{16}$$

where r is the separation between maser spots, and $\Sigma(r)$ is the surface density of companions to a given maser spot at separation r, averaged over all spots. For the realization shown in Figs 2 and 3, we found $d = 0.99$. When the fractal dimension of an object is less than 2, the dimension of a fractal residing in three-dimensional space coincides with that of its two-dimensional projection [e.g., Falconer (1990)]. Thus, the computed fractal dimension of the saturated maser output is nearly identical to the fractal dimension ($d = 1$) of the simulated turbulent activity (Section 3.1).

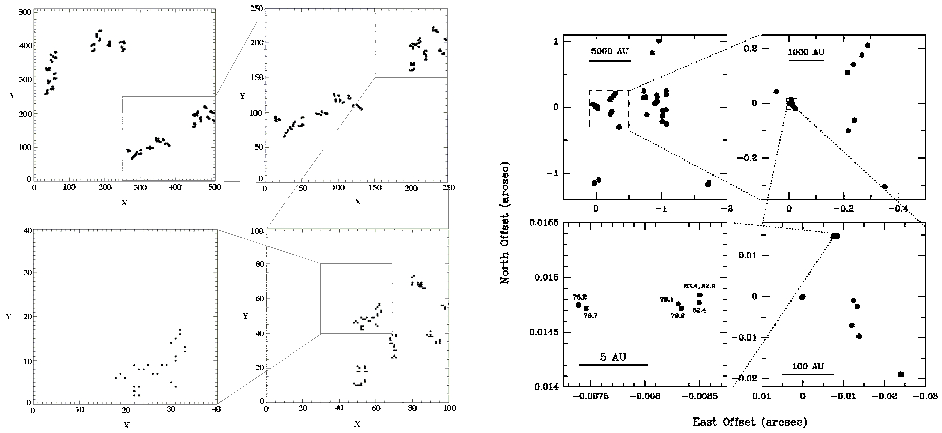


Figure 4 (*left*): Multi-scale (x, y) map of saturated maser emission for the same realization of turbulent medium as in Figs 2 and 3. (*right*): Multi-scale map of H_2O maser source in Sgr B2(M) (Strelnitski et al. 2002).

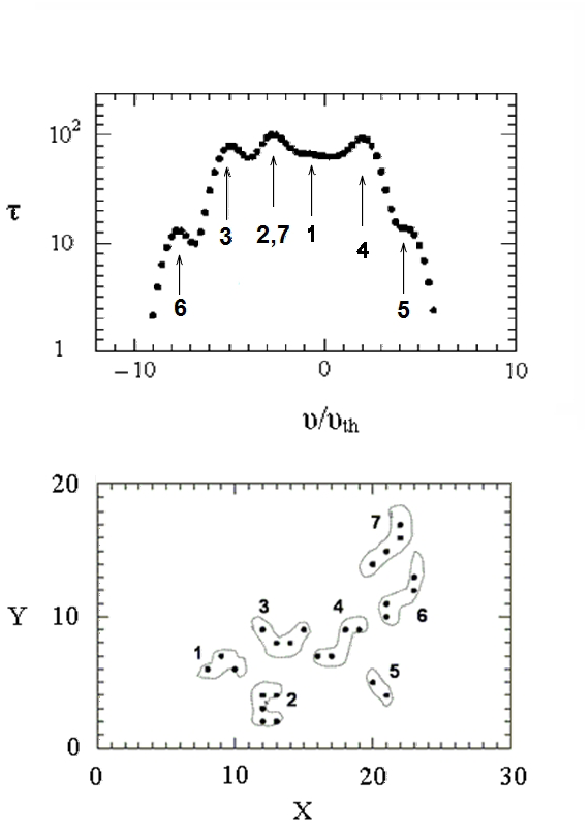


Figure 5 Spectrum and map for the smallest-scale cluster from Fig. 4 (left). Numbers indicate the groups of spots responsible for spectral features.

3.3 Comparison with observations

It is instructive to compare the obtained saturated model maps with the observed interferometric maps of strong H_2O masers associated with regions of active star formation (Fig. 4). Although the span of scales on the model map (left figure) is only slightly greater than one order of magnitude, whereas the observed map of the H_2O maser source in Sgr B2(M) (right figure) covers about three orders in scale, there is a remarkable qualitative similarity in their fractal structure.

Figure 5 shows the spectrum and the map of the smallest maser cluster in the saturated model presented in Figs 2–4. This figure can be compared with Fig. 1 of Gwinn (1994) which shows the observed spectrum and map for a smallest H_2O maser cluster in W49(N). In both cases, the smallest groups of spots, often slightly elongated and showing more or less regular velocity change along the group, are responsible for separate peaks in the integrated spectrum ("features" in Gwinn's terminology).

The only obvious difference between the observed map and the simulated map of saturated emission, Fig. 4, is the number of "observable" spots: there seem to be considerably more spots on the model map than on the observed VLBI map. Can this be an argument against the saturated and in favor of unsaturated amplification? Indeed, the number of the spots of comparable brightness is much less on the model maps of high-gain unsaturated masering than on the maps of saturated masering. Yet, the problem is that in the former case the number of the spots is *too* small (Fig. 3, right). This is in a drastic contradiction with the observations and seems to rule out a totally unsaturated amplification. The solution may, of course, be between the two extremes: a *partial* saturation.

There may be another simple explanation of why the density of spots on the simulated maps of saturated amplification are higher than on the observed maps: the different fractal dimension of these maps. The fractal dimension determined for Sgr B2(M) by the "density-radius" measure is $d = 0.44$ (Strelnitski et al. 2002), whereas for our model source $d \approx 1$. Unfortunately, because of the binary nature of the numerical arrays we use in the model, we can only create fractal sets with $d = 1$ or $d = 2$. The space filling factor p_l depends on the linear scale l as (Frish 1995):

$$p_l = \left(\frac{l}{l_0}\right)^{3-d}, \tag{17}$$

where l_0 is the largest scale. Putting $l_0 = 512$ and $l = 2$, we have $l_0/l = 256$, and from Eq. (17), the ratio of the filling factors for $d = 1$ and $d = 0.44$ is $256^{0.56} \approx 22$. Rarifying our model fractal set by a factor of 22 would certainly decrease the number of "observable" spots. It would also rarify the integral spectrum of the whole source (Fig. 1, left) and the spectrum of the smallest cluster (Fig. 4, top), making the spectral peaks more isolated, as in the observed spectra.

We also performed simulations for the case of non-intermittent turbulence, leaving all elementary cells active for masering. Such a medium produces many more "observable" hot spots on the (x, y) map for the saturated regime, and considerably more for unsaturated regime. But, of course, in contradiction with observations, there is no fractal structure of the spot distribution in either case.

We would like to emphasize that the apparent failure of the unsaturated masering to explain the observations is due to the required *high value of the gain* for H_2O masers

in star forming regions. A high gain, τ, entails a high dispersion, $\delta\tau >> 1$, which, after exponential amplification, leads to strong fluctuations of the output intensity and, as a result, a small number of very bright features dominating the spectrum and the map. For less bright maser sources, such as the 25 GHz methanol masers, which require only $\tau \approx 10$ to explain their brightness temperatures (Johnston et al. 1992), the modeling of the observations by unsaturated masering in a homogeneous (non-intermittent) turbulent medium seems to be satisfactory (Sobolev, Wallin & Watson 1998). However, other arguments indicate that these masers are probably saturated as well (Strelnitski 1981; Johnston et al. 1992).

Conclusions

Comparison of the observed spectra and VLBI maps of H_2O masers in regions of star formation with synthetic spectra and maps produced by a numerical model of maser amplification in a turbulent medium shows that only *saturated* amplification in a medium with *intermittent* turbulence (i.e., the medium causing a fractal structure of masering activity) can produce spectra and maps that are in good qualitative agreement with the observations — spectra with many overlapping peaks of comparable intensity and maps tracing a fractal structure over several orders of magnitude in scale. Unsaturated amplification in a fractal medium with a dimension $d \lesssim 1$ and with the maximum optical depth $\tau \gtrsim 30$ (both required by the observations), produces only very few bright peaks in the spectrum and very few hot spots on the map, with no detectable fractal structure.

We conclude that if the H_2O masers in regions of star formation are associated with turbulence, they are very likely to be highly saturated.

Acknowledgments We are grateful to S.V. Kalenskii for pointing out an important ambiguity regarding the optical depth of the maser in the original draft of the paper. N.N. acknowledges with gratitude the support of her participation in this study by the NSF (Research Experiences for Undergraduates) grant AST-0354056 and the Nantucket Maria Mitchell Association.

References

Deguchi, S. & Watson, W.D. 1986, ApJ 302, 750
Deguchi, S. & Watson, W.D. 1989, ApJ 340, L17
Dubinski, J., Narayan, R. & Phillips, T.G. 1995, ApJ 448, 226
Falconer, K.J. 1990, Fractal Geometry, Mathematical Foundations and Applications (Chichester: Wiley)
Fish, V.L., Gray, M., Goss, W. M. & Richards, A. M. S. 2011, MNRAS 417, 555
Frisch, U. 1995, Turbulence (Cambridge: Cambridge Univ. Press)
Goldreich, P. & Kwan, J. 1974, ApJ 190, 27
Gwinn, C. 1994, ApJ 429, 241
Imai, H., Deguchi, S. & Sasao, T. 2002, ApJ 567, 971

Johnston, K.J., Gaume, R., Stolovy, S., Wilson, T.L., Walmsley, C.M. & Menten, K.M. 1992, ApJ 385, 232
Nedoluha, G.E. & Watson, W.D. 1991, ApJ 367, L63
Reid, M.J., Schneps, M.H., Moran, J.M., Gwinn, C.R., Genzel, R., Downes, D. & Rönnäng, B. 1988, ApJ 330, 809
Sobolev, A.M., Wallin, B.K. & Watson, W.D. 1998, ApJ 498, 763
Strelnitski, V. 1981, Sov. Ast. Letters 7(4), 223
Strelnitski, V. 1982, Sov. Ast. 8, 86
Strelnitski, V. 1984, MNRAS 207, 339
Strelnitski, V., Alexander, J., Gezari, S., Holder, B.P., Moran, J.M. & Reid, M.J. 2002, ApJ 581, 1180
Walker, R.C. 1984, ApJ 280, 618
Wallin, B.K., Watson, W.D. & Wyld, H.W. 1998, ApJ 495, 774